Received May 4, 2021, accepted May 17, 2021, date of publication May 20, 2021, date of current version June 2, 2021.

Digital Object Identifier 10.1109/ACCESS.2021.3082261

Retrieving the Effective Parameters of an Electromagnetic Metamaterial Using the Nicolson-Ross-Weir Method: An Analytic Continuation Problem Along the Path Determined by Scattering Parameters

GIOVANNI ANGIULLI[1], **(Senior Member, IEEE), AND MARIO VERSACI**[2], **(Senior Member, IEEE)**

[1]Department of Information Engineering, Infrastructures and Sustainable Energy, Mediterranea University of Reggio Calabria, 89124 Reggio Calabria, Italy
[2]Department of Civil, Energetic, Environmental and Material Engineering, Mediterranea University of Reggio Calabria, 89124 Reggio Calabria, Italy

Corresponding author: Giovanni Angiulli (giovanni.angiulli@unirc.it)

ABSTRACT Electromagnetic metamaterials (MMs) are composite structures that allow one to potentially develop unique and innovative microwave, millimetre wave, and optical devices due to their unusual physical properties. In this process, their electromagnetic characterization plays a fundamental role. Various procedures have been proposed to accomplish this task, but the Nicolson-Ross-Weir (NRW) method still appears to be the most commonly adopted one even though it is afflicted by the severe issue of branch ambiguity. In this paper, we have demonstrated that rigorously, as the branch ambiguity can be entirely overcome through the analytic continuation of a specific analytic logarithm element along the path determined in the complex plane by the scattering parameters of an MM under analysis. Furthermore, the underlying relationship between analytic continuation, phase unwrapping approach, implemented through a procedure devised by Oppenheim and Schafer for the homomorphic treatment of signals (hereafter named PUNWOS), and the Kronig-Kramers relation has been discussed and enlightened, demonstrating the full equivalence among the methods. To clarify this aspect, a couple of numerical examples is presented. The results discussed in this study open the possibility of employing the vast theoretical equipment developed in the phase unwrapping field to achieve the retrieval of MMs' effective parameters when the NRW method is applicable.

INDEX TERMS Electromagnetic metamaterial, Nicolson-Ross-Weir retrieval method, branch ambiguity problem, phase unwrapping, analytic continuation, Kramers-Kronig relations.

I. LIST OF SYMBOLS

ω	Angular frequency
ϵ_{eff}	Effective dielectric permittivity
μ_{eff}	Effective magnetic permeability
N_{eff}	Effective complex refraction index
z_{eff}	Effective intrinsic impedance
S_{11}, S_{12}	Metamaterial scattering parameters
R_{01}	Reflection coefficient
κ_{eff}	Effective extinction factor
n_{eff}	Effective refractive index
k_0	Free space propagation constant
d_{eff}	Effective thickness
$LOG(\cdot)$	Complex logarithm
$log(\cdot)$	Principal logarithm
$\mathsf{Re}[\cdot]$	Real part operator
$\mathsf{Im}[\cdot]$	Imaginary part operator
$f(\cdot)$	An analytic function
$\mathbb{D}$	$f(\cdot)$'s domain
$\mathbb{C}$	Complex plane
$\dot{\mathbb{C}}$	Complex punctured plane
$f(\mathbb{D})$	$f(\cdot)$'s range
$f^{-1}(\cdot)$	Inverse of $f(\cdot)$
$\bar{\Omega}$	Sub-domain of $f(\mathbb{D})$

The associate editor coordinating the review of this manuscript and approving it for publication was Weiren Zhu.

$h(\cdot)$	Right-inverse of $f(\cdot)$
$\gamma(\cdot)$	Path in $\dot{\mathbb{C}}$
$\bar{\gamma}(\cdot)$	Path in $\mathbb{C}$
Ω	Sub-domain of $\dot{\mathbb{C}}$
$l(\cdot)$	Analytic logarithm
Ω_α	Star-domain
$log_\alpha(\cdot)$	Analytic α-logarithm
$ln(\cdot)$	Natural logarithm
$\lvert\cdot\rvert$	Absolute value function
$arg_\alpha(\cdot)$	α-argument function
z	Complex number
$Arg(z)$	Set of arguments of z
$\mathbb{Z}$	Set of the integer numbers
R, R', R_k	Sub-domains of $\mathbb{C}$
$\varnothing$	Empty set
$\sqsubset$	Subordination operator
$\mathsf{L}(\cdot)$	Unique analytic logarithm
$\triangleq$	Is defined to be equal to – symbol
$\mathbb{R}^+$	Positive real axis
$\mathcal{S}$	Homomorphic system
$\phi_{\mathcal{S}}(\cdot)$	Input-output function
$[\odot, \oplus]$	Set of the generalized input operations
$[\boxdot, \boxplus]$	Set of the generalized output operations
$\mathcal{C}$	Canonical homomorphic system
$\mathcal{H}', \mathcal{L}, \mathcal{H}''$	Canonical homomorphic sub-systems
$\phi'_{\mathcal{H}}(\cdot), \phi_{\mathcal{L}}(\cdot), \phi''_{\mathcal{H}}(\cdot)$	Input-output functions
$\circ$	Composition operator
$\mathcal{P}$	Cauchy principal value
ϵ_r	Dielectric permittivity
μ_r	Magnetic permeability
n	Refractive index

II. INTRODUCTION

Electromagnetic metamaterials (MMs) are composites that exhibit unusual physical characteristics when exposed to the action of an external electromagnetic field [1], [2]. This can potentially make the development of cutting-edge innovative microwave, millimetre wave, and optical frequency devices a real possibility, see for example [3]–[5] and references within for a detailed overview of this argument. An MM is usually created by arranging suitable identical scattering elements, the *meta-atoms*, in an appropriate lattice configuration [1]. For analysis and design purposes, the external electromagnetic behaviour of an MM is modeled by considering this structure equivalent to a continuous medium, which is called an *effective medium* (see Figure 1) and is usually characterized by an effective scalar electric permittivity $\epsilon_{eff}(\omega)$ and magnetic permeability $\mu_{eff}(\omega)$ [1], [2] where ω is the angular frequency (effective tensorial parameters are also possible, but from a conceptual point of view, the rationale is the same as the scalar case [6]). This perspective, technically defined as *homogenization procedure* [1], [2], is commonly

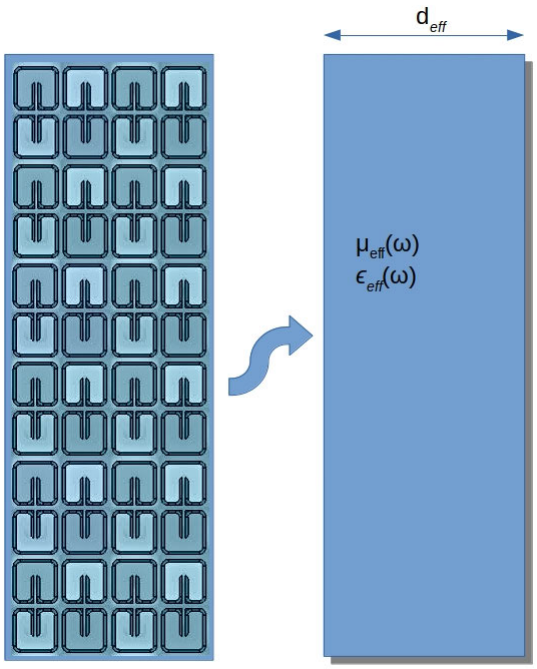

FIGURE 1. An example of a metamaterial slab and its related effective medium slab.

justified by considering that both the size of the meta-atoms and their mutual distances are far smaller in comparison with the wavelength of the external electromagnetic field [1]–[8].

The Nicolson-Ross-Weir (NRW) method [9] still appears to be the approach most commonly adopted by researchers to recover the effective constitutive parameters of these structures; see, for example, [10]–[15] and references within. By using the NRW method, the effective medium parameters are promptly evaluated through the inversion of the relation that links among them the effective complex refraction index $N_{eff}(\omega)$ to the scattering parameters (measured or simulated), thereby characterizing the MM sample under study [1], [2], [8]. Despite its straightforwardness, several limitations and inconsistencies plague this homogenization procedure, and in references [16], [17], these problems have been broadly discussed. Nevertheless, under the hypothesis that the conditions for its applicability are fully fulfilled [16], [17], the branch ambiguity problem remains the most relevant and challenging issue among all [18]. It negatively affects the unambiguous determination of the real part of $N_{eff}(\omega)$ and, as a consequence, the unambiguous determination of $\epsilon_{eff}(\omega)$ and $\mu_{eff}(\omega)$ [18], [19]. Although several methods have been proposed to overcome this problem [19]–[21], the approaches based both on the Kronig-Kramers relations [22]–[26] and the phase unwrapping approach–the latter being implemented through numerical procedures essentially derived from the algorithm developed by Oppenheim and Schafer for homomorphic filtering (hereafter named PUNWOS) [27]–are mostly employed to accomplish this task [28]–[32]. Regarding the use of Kronig-Kramers relations, it should be mentioned that these are well known, grounded in causality with $N_{eff}(\omega)$ having to be rigorously

a causal physical quantity [33], [34]. In regard to the phase unwrapping-based approach, to the best of the authors' knowledge, it seems to lack a similar logical ground despite the fact that a number of papers have exploited this method. In fact, the only type of validation for this method has been a comparison of its results with those provided by the Kroenig-Kramers approach [32], and in any case, the relationship between the two approaches does not seem to have been clarified so far [35], [36]. Hence, based on these premises, the purpose of our work was two-fold. First, we rigorously demonstrated that the branch ambiguity problem affecting the NRW method can be fully overcome and, accordingly, the complex refraction index $N_{eff}(\omega)$ can be uniquely evaluated through the careful inversion of the exponential relationship between $N_{eff}(\omega)$ and the scattering parameters of the MM at hand by the computation of a suitable right-inverse obtained through the analytic continuation of a specific analytic logarithm element along the path determined by the S-parameters in the complex plane. Second, based on this result, the rationale linking analytic continuation with the PUNWOS approach was discussed and enlightened, thereby demonstrating the full equivalence between the two approaches. Finally, this equivalence was exploited to demonstrate the relationship with the Kronig-Kramers approach. The paper is organized as follows: in section III we introduce the theoretical foundations used in our study. Since the arguments exploited for our discussion are quite scattered in the specialized literature, all the theoretical concepts needed for this aim are rigorously provided. At this purpose we divided the section into three subsections: the first one summarizes the effective constitutive parameters evaluation process provided by the NRW method and the related branch ambiguity issue. The second subsection elucidates the origin of the branch ambiguity issue and the way to overcome it. This subsection starts analyzing the mathematical relationship from which the MM's complex refraction index is obtained from an algebraic perspective. This analysis shows as the branch ambiguity issue has its roots in the intrinsic lack of "bijectivity" (under certain conditions) of the functional relation for $N_{eff}(\omega)$, and highlights as this problem can be fully overcome through the concept of right-inverse function. The third subsection shows as this right-inverse is obtained by the analytic continuation, along the path determined by the MM's scattering parameters, i.e. the curve drawn on $\mathbb{C}$ by the known term of the relationship mentioned above as a function of the angular frequency, of a suitable analytic logarithm function. Due to the intrinsic lack of uniqueness of the right-inverse, a suitable constraint condition is required to achieve this prolongation, and this point is here rigorously faced. In section IV, we discuss how the PUNWOS approach developed by Oppenheim and Schafer can be understood in terms of analytic continuation, i.e. in term of continuity of imaginary part of the prolonged analytic logarithm, and provide clarification on the relationship existing between the Kronig-Kramers relations and PUNWOS. To enlighten the theoretical machinery presented in section III and check the equivalence among methods, in section V, we present some numerical experiments conducted on two negative refractive index (NRI) media characterized by the same effective parameters but having different thickness. Finally, in section VI, we draw our conclusions and sketch future research directions.

III. THEORY

A. THE NICOLSON-ROSS-WEIR (NRW) METHOD

The NRW method is a classical technique that has been employed for decades to recover the constitutive electromagnetic parameters of linear, isotropic, and homogeneous media [9]. It was used for the first time by D. R. Smith and co-authors in [7] to characterize an MM structure that was created through a periodic arrangement of wires and split ring resonators. According to this approach, the effective electromagnetic constitutive parameters of an MM slab of finite thickness can be recovered through the solution of the following system of equations (the time-dependence $e^{-i\omega t}$ is assumed) [8]:

$$S_{11}(\omega) = \frac{R_{01}(\omega)(1 - e^{i2N_{eff}(\omega)k_0 d_{eff}})}{1 - R_{01}^2(\omega)e^{i2N_{eff}(\omega)k_0 d_{eff}}} \tag{1}$$

$$S_{21}(\omega) = \frac{(1 - R_{01}^2(\omega))e^{i2N_{eff}(\omega)k_0 d_{eff}}}{1 - R_{01}^2(\omega)e^{i2N_{eff}(\omega)k_0 d_{eff}}} \tag{2}$$

that relates the constitutive parameters of the effective medium slab that are equivalent to the MM slab at hand with the MM scattering parameters (computed or measured). In the aforementioned relations, the terms $N_{eff}(\omega)$, d_{eff}, and k_0 are the complex refraction index, the thickness of the effective medium [22], and the free-space propagation constant, respectively, while the term $R_{01}(\omega)$ where

$$R_{01}(\omega) = \frac{z_{eff}(\omega) - 1}{z_{eff}(\omega) + 1} \tag{3}$$

represents the reflection coefficient evaluated at the planar interface between the free space and the effective medium. From (1) and (2), we obtain the following:

$$z_{eff}(\omega) = \pm\sqrt{\frac{(1 + S_{11}(\omega))^2 - S_{21}^2}{(1 - S_{11}(\omega))^2 - S_{21}^2}} \tag{4}$$

$$e^{iN_{eff}(\omega)k_0 d_{eff}} = \frac{S_{21}(\omega)}{1 - S_{11}(\omega)R_{01}(\omega)} \tag{5}$$

where $z_{eff}(\omega)$ is the MM effective intrinsic impedance. The proper sign in (4) was chosen by imposing that the amplitude of the reflected field results in the lowering of the amplitude of the incident field [7], [19]. The expression of $N_{eff}(\omega)$ is obtained from (5) the following:

$$\begin{aligned} N_{eff}(\omega) &= n_{eff}(\omega) + i\kappa_{eff}(\omega) \\ &= \frac{i}{k_0 d_{eff}}\left[LOG\left(\frac{S_{21}(\omega)}{1 - S_{11}(\omega)R_{01}(\omega)}\right)\right] \\ &= \frac{i}{k_0 d_{eff}}\left[log\left(\frac{S_{21}(\omega)}{1 - S_{11}(\omega)R_{01}(\omega)}\right) + 2p\pi i\right] \end{aligned} \tag{6}$$

where $LOG(\cdot)$ and $log(\cdot)$ denote the complex [37] and the principal logarithm [37], respectively, and where the term $p = 0, \pm1, \pm2, \pm3, \ldots$ is the *branch index* [37]. The effective extinction (or attenuation) factor $\kappa_{eff}(\omega)$ and the effective refractive index $n_{eff}(\omega)$ are as follows:

$$\alpha_{eff}(\omega) = -\frac{1}{k_0 d_{eff}} \mathsf{Re}\left[log\left(\frac{S_{21}(\omega)}{1 - S_{11}(\omega)R_{01}(\omega)}\right)\right] \quad (7)$$

$$n_{eff}(\omega) = \frac{1}{k_0 d_{eff}} \mathsf{Im}\left[log\left(\frac{S_{21}(\omega)}{1 - S_{11}(\omega)R_{01}(\omega)}\right)\right] + 2p\pi i \quad (8)$$

where $\mathsf{Re}[\cdot]$ and $\mathsf{Im}[\cdot]$ are the real and the imaginary part operators [37]. From the aforementioned relations, we understand that the $\alpha_{eff}(\omega)$ results need to be uniquely determined in contrast to the term $n_{eff}(\omega)$ whose ambiguity is due to the presence of the branch index p in (8). This hinders the unambiguous electromagnetic characterization of the MM structure under analysis. Assuming for now that this issue known in literature as the *branch ambiguity problem* [18], [19] has been solved, we understand that the effective parameters can be uniquely computed as follows [22], [23]:

$$\epsilon_{eff}(\omega) = \frac{N_{eff}(\omega)}{z_{eff}(\omega)} \quad (9)$$

$$\mu_{eff}(\omega) = N_{eff}(\omega) z_{eff}(\omega) \quad (10)$$

B. INVERTING AN ABSTRACT EQUATION

To overcome the critical issue of the ambiguity plaguing the real part of the complex refraction index $N_{eff}(\omega)$ results, it is essential, although tedious, to examine the rationale of its calculation process in a comprehensive and detailed way. Hence, first, we start to consider the following abstract equation:

$$f(w) = z \quad (11)$$

where $f(\cdot)$ is an analytic function with domain $\mathbb{D}$, lying in the complex plane $\mathbb{C}$, ($w \in \mathbb{D} \subseteq \mathbb{C}$), and range $f(\mathbb{D}) \subseteq \mathbb{C}$ ($z \in f(\mathbb{D})$) [37], [38]. If the function $f(\cdot)$ in (11) is a single-valued analytic function from $\mathbb{D}$ onto $f(\mathbb{D})$, i.e., if $f(\cdot)$ is *univalent* [37], we understand that the $f(\cdot)$ results will be invertible and the relation (11) can be solved formally as follow [38]:

$$w = f^{-1}(z) \quad (12)$$

where the function $f^{-1}(\cdot)$, which is *analytic* and *unique*, is called the *inverse* of $f(\cdot)$ [38], [39]. If the univalence is not fulfilled, the inverse $f^{-1}(\cdot)$ does not exist, and the (11) cannot be solved using this concept [38], [39]. However $f(\cdot)$ can always be *right-inverted*, i.e., there exists an univalent *analytic* function $h(\cdot)$, named *right-inverse*, with domain $\bar{\Omega} \subseteq f(\mathbb{D})$ and range $\mathbb{D}$ such that:

$$f(h(z)) = z \quad \forall z \in \Omega \quad (13)$$

with $w = h(z)$ [38], [39]. Unlike the inverse function $f^{-1}(\cdot)$, the right-inverse function $h(\cdot)$ is *not unique* [38], [39]. Of course, if $f(\cdot)$ is invertible, it is also right-invertible and

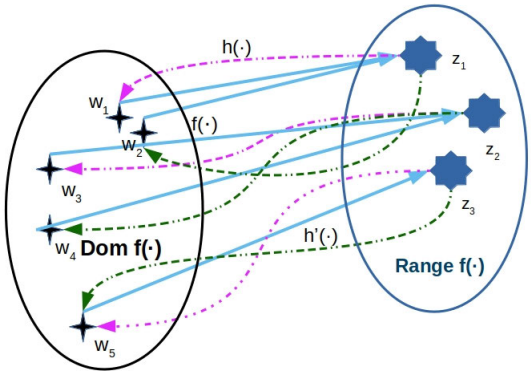

FIGURE 2. Example of a non-univalent function $f(\cdot)$ (continuous light blue line). It can be noticed that its two right-inverses $h(\cdot)$ (dotted purple line) and $h'(\cdot)$ (dotted green line) select different pre-images in the $f(\cdot)$'s domain.

$h(\cdot) = f^{-1}(\cdot)$ [38], [39]. Accordingly, if $f(\cdot)$ is non-univalent, it is impossible to obtain a unique solution from inverting (11) without using a suitable constraint condition suggested by the problem under consideration [39]. In fact, after fixing an image point $z \in \bar{\Omega}$, a particular right-inverse $h(\cdot)$ can select only one among the pre-image points w encompassed in the domain of $f(\cdot)$ [39]. This particular pre-image point w' depends exactly on which right inverse $h(\cdot)$, among all the right-inverses for $f(\cdot)$, is used to solve (11) (see Figure 2) [39], and it is the constraint condition that allows the selection of this particular right-inverse function $h(\cdot)$ from the set of all the right-inverses admissible for $f(\cdot)$ [38], [39]. In the light of the theoretical concepts discussed above, we re-examine the relation (5) more carefully. We point out that (5) can be rewritten as (11) with a simple change of variable $w = i2N_{eff}(\omega)k_0 d_{eff}$ and $z = \frac{S_{21}(\omega)}{1-S_{11}(\omega)R_{01}(\omega)}$, both terms being complex-valued functions of the variable ω and setting $f(\cdot) = e^{(\cdot)}$. The domain $\mathbb{D}$ and the range $f(\mathbb{D})$ for the complex exponential function $e^{(\cdot)}$ are the images of $i2N_{eff}(\omega)k_0 d_{eff}$, and $\frac{S_{21}(\omega)}{1-S_{11}(\omega)R_{01}(\omega)}$, respectively. It can be noticed that these domains are *paths*. These paths that we denoted as $\bar{\gamma}(\cdot)$ and $\gamma(\cdot)$ lie in the complex plane $\mathbb{C}$ and the complex punctured plane $\dot{\mathbb{C}} = \mathbb{C} - \{0\}$, respectively. From the theory of the analytic functions, we know that $e^{(\cdot)}$ is univalent only and exclusively on half-open rectilinear strips of width 2π parallel to the real axes of the complex plane $\mathbb{C}$ (see figure 3) [37]. However, as the number of strips on which $\bar{\gamma}(\cdot)$ lies is unknown (although this piece of information is closely related to the extension of the path $\gamma(\cdot)$ in $\dot{\mathbb{C}}$), we are obliged to address $e^{(\cdot)}$ as a non-univalent function and to solve (5) accordingly, as discussed in the following section.

C. COMPUTING THE PROPER RIGHT-INVERSE

In light of the theoretical concepts stated earlier, it becomes apparent that the critical point for overcoming the branch ambiguity problem and, thereby, unambiguously solving (5) lies in the computation of the proper right-inverse $h(\cdot)$ for this relation, which is indicated using the symbol $\mathsf{L}(\cdot)$. As demonstrated in the following part of this subsection,

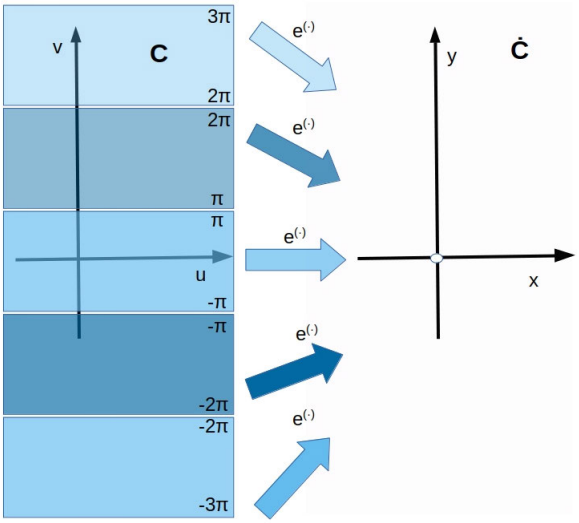

FIGURE 3. Domains of univalence for the complex exponential function $e^{(\cdot)}$ and their mapping onto the complex punctured plane $\dot{\mathbb{C}}$.

$\mathsf{L}(\cdot)$ can be built through the analytic continuation of a precisely defined analytic logarithm lying on a circular domain centered on the starting point of the path traced in $\dot{\mathbb{C}}$ by the term $\frac{S_{21}(\omega)}{1-S_{11}(\omega)R_{01}(\omega)}$, with the constraint $\mathsf{Im}(\mathsf{L}(\gamma(0))) = 0$ (we return to this point and discuss it more rigorously in subsection III-C3). Because the demonstration of this way of proceeding to evaluate $\mathsf{L}(\cdot)$ is founded on specific concepts of the analytic function theory and taking into account that the main theoretical results needed for this aim are scattered in the specialized mathematical literature on complex analysis, we collect and discuss these arguments with some degree of detail. More precisely, we start providing the concept of analytic α-logarithm (sub-subsection III-C1), followed by some basics on analytic continuation (sub-subsection III-C2). Next, the path covering lemma is introduced (sub-subsection III-C2). On this result is grounded the fundamental Theorem 1 from which an algorithm for computing $\mathsf{L}(\cdot)$ is derived (sub-subsection III-C3).

1) ANALYTIC α-LOGARITHMS

We start considering an analytic function $h(\cdot)$ with domain $\Omega \subset \dot{\mathbb{C}}$ and range $\mathbb{C}$ such that

$$e^{h(z)} = z \quad \forall z \in \Omega. \tag{14}$$

The right-inverse function $h(\cdot)$ indicated in the following as $l(\cdot)$ is called an *analytic logarithm* on Ω [38], [40]. As a consequence of the periodicity of the complex exponential function [37], any function of the form $l'(\cdot) = l(\cdot)+2p\pi i$ with $p \in \mathbb{Z}$ is also an analytic logarithm on Ω [38], [40], i.e., on Ω, there exist *infinite* right inverses for (14). Henceforth, we consider for our purposes the domains Ω of the type $\Omega_\alpha = \mathbb{C}-\mathbb{R}_\alpha$, named *star-domains*, where $\mathbb{R}_\alpha = \{\rho e^{i\alpha} \in \mathbb{C}, \rho \geq 0\}$ is a ray starting from the origin of $\mathbb{C}$ and forming an angle $\alpha \geq 0$ with its positive real semi-axis (see figure 4) [40].

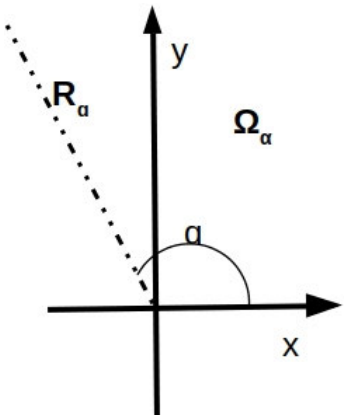

FIGURE 4. A typical Star-Domain Ω_α.

An analytic logarithm $l(\cdot)$ of the following form:

$$log_\alpha(\cdot) = ln(|\cdot|) + i[arg_\alpha(\cdot)] \tag{15}$$

where $ln(\cdot)$ is the natural logarithm [37], $|\cdot|$ is the absolute value function [37], and $arg_\alpha(\cdot)$ is the α-argument function defined as follows [40]:

$$arg_\alpha(\cdot) = \{\forall z \in \Omega_\alpha, arg_\alpha(z) = Arg(z) \cap (\alpha - 2\pi, \alpha]\} \tag{16}$$

where $Arg(z)$ is a set of the following arguments:

$$Arg(z) = \left\{\theta \in \mathbb{R} : z = |z|e^{i\theta}, z \in \mathbb{C}\right\} \tag{17}$$

is called *analytic α-logarithm* on Ω_α [40]. Accordingly, because every analytic logarithm $l'(\cdot)$ defined on Ω_α can be written as follows [40]:

$$l'(\cdot) = log_\alpha(\cdot) + i[arg_\alpha(\cdot) + 2p\pi], \quad p \in \mathbb{Z}. \tag{18}$$

we can state that $log_\alpha(\cdot)$ is the *principal logarithm* on Ω_α, i.e., the *root* from which all the others logarithms on this domain are derived [40].

2) ANALYTIC CONTINUATION

The expansion of the original domain of the definition $\mathbb{D} \subset \mathbb{C}$ of an univalent function $f(\cdot)$ onto a larger domain of the complex plane is called *analytic continuation* (of $f(\cdot)$) [37], [38]. To explain how this process can be carried out, we need to provide a few preliminary definitions. An *analytic function element* is a couple $(f(\cdot), R)$ where $f(\cdot)$ is the analytic function and R is a domain in $\mathbb{C}$ [37], [38]. If the domain R is an open disk D, the couple $(f(\cdot), D)$ is called *circular analytic function element* [37]. Two analytic function elements $(f(\cdot), R)$ and $(f'(\cdot), R')$ are considered identical if and only if we have $f(\cdot) = f'(\cdot)$ and $R = R'$. Now, an analytic function element $(f(\cdot), R)$ is the *direct analytic continuation* of another analytic function element $(f'(\cdot), R')$ in case of the following [37]:

$$R \cap R' \neq \varnothing \tag{19}$$

$$\exists \Psi \subset R \cap R' : f(z) = f'(z) \quad \forall z \in \Psi \tag{20}$$

From the definition provided above, it follows that $f(\cdot)$ and $f'(\cdot)$ can be regarded as the particular representation of an analytic function $F(\cdot)$ defined as follows [37], [38]:

$$F(z) = \begin{cases} f(z) & \forall z \in R \\ f'(z) & \forall z \in R' \end{cases} \tag{21}$$

with domain $\mathbb{D} = R \cup R'$. An analytic function element (f, R) is called *subordinate* to another analytic function element (f', R'), i.e., $(f, R) \sqsubset (f', R')$, in case of the following [37]:

$$R \subset R' \tag{22}$$

$$f(z) = f'(z) \quad \forall z \in R. \tag{23}$$

It is easy to note that if $(f, R) \sqsubset (f', R')$, the first analytic element is a direct analytic continuation of the second one [37]. A set of the following elements:

$$\{(f_0(\cdot), R_0), (f_1(\cdot), R_1), \ldots, (f_n(\cdot), R_n)\} \tag{24}$$

where the analytic element $(f_k(\cdot), R_k)$ is a direct analytic continuation of the analytic element $(f_{k-1}(\cdot), R_{k-1})$ for $k = 1, 2, \ldots, n$ is called *chain of analytic function elements* [37]. The first and last elements of this chain, $(f_0(\cdot), R_0)$ and $(f_n(\cdot), R_n)$, respectively, are the *indirect analytic continuation* or, more simply, the *analytic continuation* of each other. As an analogy for direct analytic continuation between a couple of elements, the chain of analytic function elements can also be regarded as the representation of an analytic function $F(\cdot)$ [37]:

$$F(\cdot) = \begin{cases} f_0(z) & \forall z \in R_0 \\ \vdots & \\ f_n(z) & \forall z \in R_n \end{cases} \tag{25}$$

defined on the domain $\mathbb{D} = R_0 \cup \cdots \cup R_n$. The analytic continuation of an analytic function element $(f(\cdot), R)$ is also possible along a continuous path $\gamma(\cdot)$ of the complex plane $\mathbb{C}$. The following theorem is of paramount importance for establishing this result [41]:

Path Covering Lemma: Let $\gamma : [a, b] \to \mathbb{C}$ be a continuous path. We know that

- The domain of $\gamma(\cdot)$ can always be subdivided as $t_0 < t_1, \ldots, < t_n$ with $t_0 = a$ and $t_n = b$ so that every $\gamma(t_k)$, $k = 0, \ldots, n$ is at the center of the open disk D_k;
- Each sub-path of $\gamma(\cdot)$ lying between the center $\gamma(t_{k-1})$ and $\gamma(t_{k+1})$ is contained in the open disks D_k as follows:

$$\begin{aligned} &\gamma(t) \subset D_0, \quad t \in [t_0, t_1]; \\ &\gamma(t) \subset D_k, \quad t \in [t_{k-1}, t_{k+1}], \ k = 1, \ldots, n-1; \\ &\gamma(t) \subset D_n, \quad t \in [t_{n-1}, t_n]; \end{aligned}$$

- The radii of the disks D_k can be chosen to be i) of the same size (if necessary) and ii) arbitrarily small.

In sum, the Path Covering Lemma states that an arbitrary $\gamma(\cdot)$ lying in $\mathbb{C}$ can always be covered by a finite set of n overlapping open disks, thereby realizing a *chain of domains* in $\mathbb{C}$ embedding this path (see figure 5). In this way, the analytic continuation of an analytic function element (f, D) along $\gamma(\cdot)$ can be accomplished following the same principles used to prolong an arbitrary analytic function element along $\mathbb{C}$ [37].

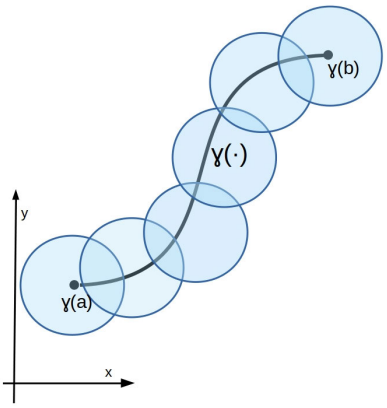

FIGURE 5. Example of paving for a path $\gamma(\cdot)$ in $\mathbb{C}$.

3) THE UNIQUE ANALYTIC LOGARITHM ON A PATH $\gamma(\cdot)$

Now, we are in condition to provide the central result on which is based our approach for overcoming the branch ambiguity in the NRW method:

Theorem 1: Let $\gamma : [a, b] \to \dot{\mathbb{C}}$ be a continuous path. There exists a unique analytic logarithm $\mathsf{L}(\cdot)$ such that

$$e^{\mathsf{L}(z)} = z \quad \forall z \in \gamma(t) \quad t \in [a, b] \tag{26}$$

fulfilling the constraint condition $\mathsf{Im}(\mathsf{L}(\gamma(a))) = \theta_0$ with $\theta_0 \in \mathbb{R}$ and $e^{i\theta_0} = \frac{\gamma(a)}{|\gamma(a)|}$.

Existence - Because of the path covering lemma, we know that $\gamma(\cdot)$ can be paved by a finite set of n overlapped open disks $D_0, \ldots, D_n$. Each disk $D_k, k = 0, \ldots, n$ is a subset of a specific domain[1] $\Omega_{\alpha_k} \subset \dot{\mathbb{C}}$. On each D_k, a circular analytic function element of the form $(log_{\alpha_k}, D_k) \sqsubset (log_{\alpha_k}, \Omega_{\alpha_k})$ can be defined so that the path $\gamma(\cdot)$ results are embedded in the cluster of circular analytic logarithm elements (log_{α_k}, D_k), $k = 0, \ldots, n$. In correspondence of centre $\gamma(a)$ of the open disk D_0, we enforce:

$$e^{(log_{\alpha_0}(\gamma(a)))} = \gamma(a) = |\gamma(a)| e^{i\theta_0} \tag{27}$$

where $\mathsf{Im}(log_{\alpha_0}(\gamma(a))) = arg_{\alpha_0}(\gamma(a))$ can coincide with the phase of $\gamma(a)$, θ_0 or differ by a multiple of 2π. In this last case, by adding to $log_{\alpha_0}(\gamma(a))$ the term $2p_0\pi i$ with p_0 an appropriate integer, we can obtain the phase-matching we want to enforce. Accordingly, we now have the following equation:

$$log'_{\alpha_0}(\cdot) = log_{\alpha_0}(\cdot) + 2p_0\pi i \tag{28}$$

on D_0. Considering the open disks D_0 and D_1, we know that

$$e^{(log'_{\alpha_0}(z))} = z \quad \forall z \in \gamma(t) \quad \gamma(t) \subset D_0 \quad t \in [t_0, t_1] \tag{29}$$

[1]This can be demonstrated in the following way: let $\mathbb{R}_\alpha$ for a suitable choice of α and the ray orthogonal to the line segment $[0, \gamma(t_k)]$. Accordingly, the open disk D_k has to belong to one of the two open half planes of Ω_α.

$$e^{(log_{\alpha_1}(z))} = z \quad \forall z \in \gamma(t) \quad \gamma(t) \subset D_1 \quad t \in [t_1, t_2] \tag{30}$$

At $z_1 = \gamma(t_1) \in D_0 \cap D_1$, we must have the following:

$$e^{log'_{\alpha_0}(z_1)} = e^{log_{\alpha_1}(z_1)} \tag{31}$$

from which results the following:

$$log'_{\alpha_0}(z_k) = log_{\alpha_1}(z_1) + 2p_1\pi i \tag{32}$$

for an appropriate integer p_1. Placing $log'_{\alpha_1}(\cdot) = log_{\alpha_1}(\cdot) + 2p_1\pi i$ on D_1 and noting that $\gamma(t_j) \in D_j \cap D_{j+1}\, j \in 1, \ldots, n-1$, we can proceed between the disks D_1 and D_2 in the same way we have proceeded between the disks D_0 and D_1, thereby obtaining the following at $z_2 = \gamma(t_2)$:

$$log'_{\alpha_1}(z_2) = log_{\alpha_2}(z_2) + 2p_2\pi i \tag{33}$$

for an appropriate integer p_2. Continuing inductively on the remaining couples of disks and selecting all p_k as done previously, we obtain the following chain of circular analytic elements:

$$\{(log_{\alpha_0}(\cdot) + 2p_0\pi i, D_0), (log_{\alpha_1}(\cdot) + 2p_1\pi i, D_1), \ldots, , \ldots, (log_{\alpha_n}(\cdot) + 2p_n\pi i, D_n)\} \tag{34}$$

which defines the analytic logarithm $\mathsf{L}(\cdot)$:

$$\mathsf{L}(\cdot) = \begin{cases} log_{\alpha_0}(\cdot) + 2p_0\pi i & \forall z \in D_0 \\ log_{\alpha_1}(\cdot) + 2p_1\pi i & \forall z \in D_1 \\ \vdots & \\ log_{\alpha_n}(\cdot) + 2p_n\pi i & \forall z \in D_n \end{cases} \tag{35}$$

on the domain $\dot{\Omega} = D_0 \cup D_1 \cup \ldots D_{n-1} \cup D_n \subset \dot{\mathbb{C}}$, i.e., *i*) solution of (26) and *ii*) has the property that $\mathsf{Im}(L(\gamma(a))) = \theta_0$.

Uniqueness - Let us assume that another analytic logarithm $\mathsf{L}'(\cdot)$ on $\dot{\Omega}$, which is solution of (26), exists. Accordingly, we must know that $\mathsf{L}(\cdot)$ and $\mathsf{L}'(\cdot)$ can differ only by an integer multiple $q \in \mathbb{Z}$ of $2\pi i$ at every point of $z \in \dot{\Omega}$. In particular, in correspondence of the point $z_0 = \gamma(a)$, we must get the following:

$$\mathsf{Im}(\mathsf{L}(z_0)) = \mathsf{Im}(\mathsf{L}'(z_0)) \tag{36}$$

which implies $q = 0$. Accordingly, we must have $\mathsf{L}'(\cdot) = \mathsf{L}(\cdot)$ on $\dot{\Omega}$ $\square$.

Now, we return to (5). To obtain the unique *meaningful* solution of this relation, the constraint $\mathsf{Im}(\mathsf{L}(\gamma(a))) = \theta_0$ must specialize as follows:

$$\mathsf{Im}[\mathsf{L}(\gamma(0)] = 0 \quad (a = \omega_0 = 0) \tag{37}$$

This choice is derived from the fact that having to be the term $N_{eff}(\omega)$ the Fourier transforms of a time domain physical quantity [34], the terms

$$\gamma(t) \triangleq \frac{S_{21}(\omega)}{1 - S_{11}(\omega)R_{01}(\omega)} \tag{38}$$

and

$$\mathsf{L}(\gamma(t)) = \mathsf{L}\left(\frac{S_{21}(\omega)}{1 - S_{11}(\omega)R_{01}(\omega)}\right) \tag{39}$$

must be Fourier transforms quantities obeying at the same rule [42]. Specifically, from (35)

$$\mathsf{Re}[\mathsf{L}(\cdot)] = ln|\cdot| \quad \forall z \in \dot{\Omega}$$

$$\mathsf{Im}[\mathsf{L}(\cdot)] = arg(\cdot) = \begin{cases} arg_{\alpha_\pi}(\cdot) + 2p_0\pi i & \forall z \in D_0 \\ arg_{\alpha_1}(\cdot) + 2p_1\pi i & \forall z \in D_1 \\ \vdots & \\ arg_{\alpha_n}(\cdot) + 2p_n\pi i & \forall z \in D_n \end{cases}$$

and $\gamma(t) \in \dot{\Omega}$ we know that

$$\mathsf{Re}\left[\mathsf{L}(\gamma(t))\right] = ln\left|\frac{S_{21}(\omega)}{1 - S_{11}(\omega)R_{01}(\omega)}\right| \tag{40}$$

is already an even function ($f(\omega) = f(-\omega)$), while only imposing (37):

$$\mathsf{Im}\left[\mathsf{L}(\gamma(t))\right] = arg\left(\frac{S_{21}(\omega)}{1 - S_{11}(\omega)R_{01}(\omega)}\right) \tag{41}$$

will result in it being an odd function ($f(\omega) = -f(-\omega)$) as it must be if we want to ensure the required property. From the above considerations, we can say that the starting point of the path $\gamma(0)$ must lie on the real positive axis. In fact, from (5), descends the following:

$$e^{(\mathsf{Re}[\mathsf{L}(\gamma(0)] + i\mathsf{Im}[\mathsf{L}(\gamma(0)])} = \gamma(0) \tag{42}$$

but

$$\mathsf{Im}[\mathsf{L}(\gamma(0))] = 0 \tag{43}$$

Accordingly, from (27) and taking into account that $\mathsf{Re}[\mathsf{L}(\gamma(t))]$ is an even (and continuous) function, we must have that

$$e^{\mathsf{Re}[\mathsf{L}(\gamma(0)]} = |\gamma(0)| = \gamma(0) \in \mathbb{R}^+ \tag{44}$$

This implies that as first element of the chain that realizes the analytic continuation, we have to select the principal logarithm $log(\cdot) = ln|\cdot| + i[arg_\pi(\cdot)]$ being $\gamma(0) \in \Omega_\pi = \mathbb{C} - \mathbb{R}_\pi$.

From Theorem 1, it is possible to derive straight away an algorithm for calculating the values of the function $\mathsf{L}(\cdot)$ on a set of samples $\{\gamma(t_k)\}_{k=0}^n \in \gamma(t)$ that are the centers of the disks $D_0, \ldots, D_n$ paving $\gamma(t)$, forcing the condition $\mathsf{Im}(\mathsf{L}(0)) = 0$. The algorithm is composed by following the steps reported in Table (1). We point out that the analytic continuation described in Theorem 1 is executed by the algorithm by forcing the continuity of the imaginary part of $\mathsf{L}(\cdot)$. To accomplish this task, the algorithm needs to evaluate and match with each other as many argument functions $arg_{\alpha_j}(\cdot), j = 0, \ldots, n$ as the number of sample points the procedure used for paving $\gamma(t)$. Although this approach is unhandy from a computational point of view, it allows the enlightening of the formal identity existing between the analytic continuation of the circular analytic element $(log(\cdot), D_0)$

Algorithm 1 Algorithm From Theorem 1

1: **procedure** Analytic Continuation
2: $\gamma(t) \triangleq \frac{S_{21}(\omega)}{1-S_{11}(\omega)R_{01}(\omega)}$, $t_0 = 0$;
3: Build on $\gamma(t)$ an admissible paving $D_0, \ldots, D_n$ by obtaining a set of samples $\{\gamma(t_k)\}_{k=0}^{n} \in \gamma(t)$;
4: Build on each disk $D_k, k = 0, \ldots, n$ an admissible $arg_{\alpha_k}(\cdot)$;
5: Compute the value of $\mathbf{L}(\gamma(a)) = ln|\gamma(a)| + i[arg_{\pi}(\gamma(a))]$; $p_0 = 0$;
6: For each $k = 1, \ldots, n$, evaluate $p_k = (arg'_{\alpha_{k-1}}(\gamma(t_k)) - arg_{\alpha_k}(\gamma(t_k)))/2\pi$ and compute the value of $\mathbf{L}(\gamma(t_k)) = ln|\gamma(t_k)| + i[arg'_{\alpha_k}(\gamma(t_k))]$ where $arg'_{\alpha_k}(\cdot) = arg_{\alpha_k}(\cdot) + 2\pi p_k$;
7: **end procedure**

centered on $\gamma(0)$ and the continuity of its argument function $arg_{\pi}(\cdot)$ over $D_0 \cup \cdots \cup D_n$ for building the analytic logarithm $\mathbf{L}(\cdot)$. However, as we will demonstrate in the next section, a better algorithmic approach to achieve the continuity of $\mathbf{Im}[\mathbf{L}(\cdot)]$, which exploits one argument function, is provided by the PUNWOS method [27].

IV. THE RELATIONSHIPS BETWEEN ANALYTIC CONTINUATION, PUNWOS, AND THE KRONIG-KRAMERS RELATIONS

In this subsection, we will demonstrate the full equivalence between the analytic continuation described in Theorem 1 and the PUNWOS approach. This will be accomplished by showing that the problem of homomorphic filtering for which PUNWOS has been introduced can be re-conducted to relation (26) and that PUNWOS is nothing more than a technique to force the continuity of $\mathbf{Im}[\mathbf{L}((\cdot)]$ by fulfilling the constraint $\mathbf{Im}[\mathbf{L}((0)] = 0$. To face these issues, it will be necessary to discuss them in a deep (and maybe tedious) way to clarify our demonstrative reasoning's underlying rationale.

A. RELATIONSHIP BETWEEN PUNWOS AND ANALYTIC CONTINUATION: HOMOMORPHIC SYSTEMS AND THE PRINCIPLE OF GENERALIZED LINEAR SUPERPOSITION

Oppenheim and Schafer introduced PUNWOS in the homomorphic signal processing context, i.e., as a nonlinear technique for handling multiplied and convolved signals [43]. For our purposes, it is necessary to recall the concepts of homomorphic system and generalized linear superposition and relate them to the mathematical model (26). We start considering a black-box system $\mathcal{S}$ characterized by *i*), an input-output relationship described by a suitable function $\phi_{\mathcal{S}}(\cdot)$ and *ii*) two sets of binary operations. The first one, $[\odot, \oplus]$, called *input operations set*, encompasses, respectively, a binary operation of *input generalized sum* $\oplus$ between a pair of arbitrary admissible input elements $\xi_i(\tau)$, $\xi_j(\tau)$, and a binary operation of *input generalized multiplication* $\odot$ between an arbitrary scalar c (real or complex) and an arbitrary admissible input element $\xi_i(\tau)$. The second one, $[\boxdot, \boxplus]$, called *output operations set*, encompasses the binary operations of *output generalized sum* $\boxplus$ and *output generalized multiplication* $\boxdot$, respectively, which operate on arbitrary scalars c and output function elements $\phi_S(\xi_i(\tau))$, $\phi_S(\xi_j(\tau))$. By using the aforementioned definitions, the *principle of general linear superposition* for $\mathcal{S}$ reads as follows [43]:

$$\phi_{\mathcal{S}}\left(c \odot \xi_i(\tau) \oplus \xi_j(\tau)\right) = c \boxdot \phi_{\mathcal{S}}(\xi_i(\tau)) \boxplus \phi_{\mathcal{S}}(\xi_j(\tau)) \quad (45)$$

A system that obeys (45) is called a *homomorphic system*. A *homomorphic class* is specifically assigned a couple of input-output operation sets $\{[\oplus, \odot], [\boxplus, \boxdot]\}$ [43]. A system falling in a given class can always be represented in a special form called *canonical*, $\mathcal{C}$, consisting of the cascade of three homomorphic systems in order from input to output: $\mathcal{H}'$, $\mathcal{L}$, and $\mathcal{H}''$. For the input system $\mathcal{H}'$, the (45) specializes as follows:

$$\phi_{\mathcal{H}'}\left(c \odot \xi_i(\tau) \oplus \xi_j(\tau)\right) = c \cdot \phi_{\mathcal{H}'}(\xi_i(\tau)) + \phi_{\mathcal{H}'}(\xi_j(\tau)) \quad (46)$$

where $\cdot$ and $+$ denote the classical binary operations of sum between functions and multiplication between a function and a scalar, and $\phi_{\mathcal{H}'}(\cdot)$ is the $\mathcal{H}'$'s input-output relationship. For the middle system, $\mathcal{L}$, which is a linear system described by the function $\phi_{\mathcal{L}}(\cdot)$, the (45) reads as follows:

$$\phi_{\mathcal{L}}\left(c \cdot \zeta_i(\tau) + \zeta_j(\tau)\right) = c \cdot \phi_{\mathcal{L}}(\zeta_i(\tau)) + \phi_{\mathcal{L}}(\zeta_j(\tau)) \quad (47)$$

where $\zeta_i(\tau) = \phi_{\mathcal{H}'}(\xi_i(\tau))$ and $\zeta_j(\tau) = \phi_{\mathcal{H}'}(\xi_j(\tau))$. Finally, for the output system $\mathcal{H}''$, the (45) results are as follows:

$$\phi_{\mathcal{H}''}\left(c \cdot \kappa_i(\tau) + \kappa_j(\tau)\right) = c \boxdot \phi_{\mathcal{H}''}(\kappa_i(\tau)) \boxplus \phi_{\mathcal{H}''}(\kappa_j(\tau)) \quad (48)$$

where $\kappa_i(\tau) = \phi_{\mathcal{L}}(\zeta_i(\tau))$, $\kappa_j(\tau) = \phi_{\mathcal{L}}(\zeta_j(\tau))$, and $\phi_{\mathcal{H}''}$ is the $\mathcal{H}''$'s input-output function. The overall input-output function for $\mathcal{C}$, $\phi_{\mathcal{C}}(\cdot)$, will be given by the composition $\circ$ of $\phi_{\mathcal{H}''}$, $\phi_{\mathcal{L}}$, and $\phi_{\mathcal{H}'}$:

$$\phi_{\mathcal{C}}(\cdot) = (\phi_{\mathcal{H}''} \circ \phi_{\mathcal{L}} \circ \phi_{\mathcal{H}'})(\cdot) \quad (49)$$

In the context of homomorphic signal processing, the class of the multiplicative homomorphic systems is of paramount importance [43]. This class is described by the property that $[\oplus, \odot] = [\boxdot, \boxplus] = [\cdot, (\cdot)^c]$ where the first operation, $\cdot$, is the standard multiplication between functions, while the second one, $(\cdot)^c$, is the standard operation of raising to the power c. In this case, we know that (45) specializes for $\mathcal{H}'$ as follows:

$$\phi_{\mathcal{H}'}\left((\xi_i(\tau))^c \cdot \xi_j(\tau)\right) = c \cdot \phi_{\mathcal{H}'}(\xi_i(\tau)) + \phi_{\mathcal{H}'}(\xi_j(\tau)) \quad (50)$$

while for $\mathcal{H}''$, we know that

$$\phi_{\mathcal{H}''}\left(c \cdot \kappa_i(\tau) + \kappa_j(\tau)\right) = (\phi_{\mathcal{H}''}(\kappa_i(\tau)))^c \cdot \phi_{\mathcal{H}''}(\kappa_j(\tau)) \quad (51)$$

To understand the relationship that must exist between $\phi_{\mathcal{H}'}(\cdot)$ and $\phi_{\mathcal{H}''}(\cdot)$, for simplicity of reasoning, we put $\phi_L(\cdot) = \mathbf{id}(\cdot)$ where $\mathbf{id}(\cdot)$ is the identity function ($\kappa_i(\tau) = \mathbf{id}(\zeta_i(\tau)) = \zeta_i(\tau)$ and $\kappa_j(\tau) = \mathbf{id}(\zeta_j(\tau)) = \zeta_j(\tau)$). Accordingly, (49) becomes the following:

$$\phi_{\mathcal{C}}(\cdot) = (\phi_{\mathcal{H}''} \circ \phi_{\mathcal{H}'})(\cdot) \quad (52)$$

If we consider as admissible the input functions $\xi_i(\tau), \xi_j(\tau)$ for the set of the real-valued functions $\mathcal{C}$ of the real variable t and only real numbers as admissible for scalars c, we can use as $\phi_{\mathcal{H}'}(\cdot)$ and $\phi_{\mathcal{H}''}(\cdot)$ the real logarithmic $ln(\cdot)$ and the exponential $e^{(\cdot)}$ functions [43]. Accordingly, the relation (45) becomes as follows:

$$e^{(ln((\xi_i(\tau))^c \cdot ln(\xi_j(\tau))))} = (\xi_i(\tau))^c \cdot (\xi_j(\tau)) \tag{53}$$

i.e., $[\oplus, \odot] = [\boxdot, \boxplus] = [\cdot, (\cdot)^c]$ as expected for a multiplicative system. Following [43], we point out that in this particular case, the inverse of $\phi''_{\mathcal{H}}(\cdot)$ being $\phi_{\mathcal{H}'}(\cdot)$, it guarantees both the identity of the input-output operations sets and the uniqueness of the results provided by the binary operations, thereby ensuring the correctness of the input-output processing. If we broaden the collection of the admissible inputs for $\mathcal{C}$ by assuming that the functions $\xi_i(\tau)$, $\xi_j(\tau)$ can be complex-valued real functions of the variable t and that the scalars c can be complex numbers, the situation is a bit quite different because in this case, $ln(\cdot)$ and $e^{(\cdot)}$ must be replaced by the complex counterparts [43]. In their seminal paper on homomorphic filtering [43], Oppenheim, Schafer, and Stockham argued for this latter case: "*If we attempt to employ the complex logarithm function as the characteristic system*" (i.e., as $\phi_{\mathcal{H}'}(\cdot)$) "*in this situation, we encounter the immediate dilemma that the output $s(\tau)$ of that system is not unique.*"(i.e., the output of $\mathcal{C}$) "*The standard artifice of invoking the principal value of the complex logarithm cannot be used in this case because the principal value of the logarithm of a product of complex signals is not always the sum of the principal values corresponding to the individual complex signals, violating (8)*" (i.e., (53)). To overcome this problem, Oppenheim and Schafer developed the PUNWOS approach [27]. PUNWOS ensures the uniqueness of the output operations by imposing the continuity of the argument of the principal logarithm $log(\cdot) = ln|\cdot| + i[arg_\pi(\cdot)]$ they chose as the complex counterpart of $ln(\cdot)$, thereby fulfilling the constraint $\mathsf{Im}(log(0)) = 0$ [44] in a way that $log(\cdot)$ can work as the inverse of the complex exponential function $e^{(\cdot)}$. More specifically, in regard to the continuity of the complex logarithm's argument $\mathsf{Im}(log(\cdot)) = arg_\pi(\cdot)$, PUNWOS works by avoiding its jumps and computing the value of the integer parameter p, which is needed to compensate the 2π discontinuity caused by crosses with the $log(\cdot)$ branch-cut (i.e., the crosses with the ray $\mathbb{R}_\pi$) when required [27], [44]. At this point, we are able to fully enlighten the relationship between the analytic continuation method and the PUNWOS approach, recasting the latter in the language employed in the subsections III-C1, III-C2, III-C3 to guarantee the uniqueness of the output operations of a multiplicative homomorphic system. First, it becomes necessary that the function $\phi_{\mathcal{H}'}(\cdot)$ turns out to be an admissible right-inverse function $l(\cdot)$ for the complex exponential function $e^{(\cdot)}$, i.e., $\phi_{\mathcal{H}'}(\cdot)$ must be an admissible solution of (14), as it is the complex logarithm $LOG(\cdot)$ a multi-valued function and, accordingly, unsuitable for this task. But this condition alone is not sufficient to satisfy the uniqueness of the results of the binary operations; it is necessary to rely on a suitable constraint for $\phi_{\mathcal{H}'}(\cdot)$, and in this case, $arg(\phi_{\mathcal{H}''}(0)) = 0$. Accordingly, $\phi_{\mathcal{H}'}(\cdot)$ must be the solution of the relation (26) under the constraint $\mathsf{Im}\left(\mathsf{L}(0)\right) = 0$. This is computed using the PUNWOS approach in the process discussed above.

B. RELATIONSHIP BETWEEN PUNWOS AND KRONIG-KRAMERS RELATIONS: AN APPLICATION OF THEOREM 1

As mentioned in section (II), the PUNWOS method and the algorithmic versions based on it have been employed in several works [28]–[30], [32]. However, without a rigorous demonstration of its validity and applicability but by simply (sometimes) comparing the provided numerical results with those given by the Kronig-Kramers relations [32], that is the *gold standard* concerning the issue of the NRW's branch ambiguity [26], [34], [36]. This section clarifies the relationship between these approaches through the theoretical results demonstrated in subsection III-C3. We start by pointing out that the terms forming the right side of the equation (5), i.e., $\gamma(t)$, are the Fourier transform of real and causal counterparts in the time domain (as they must be) [34], [45]. From Theorem 1, we know that $\mathsf{L}(\gamma(t))$ is the unique solution of (5) under the constraint (28), which is also the Fourier transform of a time-domain physical quantity (which must be causal in this case). Concerning the Kronig-Kramers relations, let us consider the following:

$$\mathsf{L}'(\gamma(t)) = \mathsf{Re}[\mathsf{L}'(\gamma(t))] + i\mathsf{Im}[\mathsf{L}'(\gamma(t))]$$

as the solution of (5) computed by using this approach. It can be evaluated as follows: from (5) and (38), we know that

$$\mathsf{Re}[\mathsf{L}'(\gamma(t))] = ln\left|\frac{S_{21}(\omega)}{1 - S_{11}(\omega)R_{01}(\omega)}\right| \tag{54}$$

The effective extinction factor $\kappa_{eff}(\omega)$ results:

$$\kappa_{eff}(\omega) = -\frac{1}{k_0 d_{eff}} ln\left|\frac{S_{21}(\omega)}{1 - S_{11}(\omega)R_{01}(\omega)}\right| \tag{55}$$

By using the Kramers-Kronig relations, the effective refractive index $n_{eff}(\omega)$ is given by [22], [34]:

$$n_{eff}(\omega) = 1 + \frac{2}{\pi}\mathcal{P}\int_0^{+\infty} \frac{\omega'\kappa(\omega')}{\omega'^2 - \omega^2} d\omega' \tag{56}$$

Finally, for the imaginary part of $\mathsf{L}(\gamma(t))$, we obtain

$$\mathsf{Im}[\mathsf{L}'(\gamma(t)] = k_0 d_{eff} n_{eff}(\omega) \tag{57}$$

From (40) and (54), we have:

$$\mathsf{Re}[\mathsf{L}'(\gamma(t))] = \mathsf{Re}[\mathsf{L}(\gamma(t))] \tag{58}$$

and taking into account that the integral (56) provides a unique solution for $\mathsf{Im}[\mathsf{L}'(\gamma(t))]$ [42], we can say that the two solutions of (5), $\mathsf{L}(\gamma(t))$ and $\mathsf{L}'(\gamma(t))$, respectively, must coincide [37]). Accordingly, the Kronig-Kramers relation and the PUNWOS approach provide, from a theoretical point of view, the same solution for $n_{eff}(\omega)$.

TABLE 1. Values of the parameters for the Lorentzian models (59),(60).

ϵ_s	static dielectric permittivity	1.2
ϵ_∞	high-frequency dielectric permittivity	1
ω_{oe}	dielectric resonance angular frequency	$2\pi \cdot 9.5$ GHz
γ_e	dielectric damping factor	0.5 GHz
μ_s	static magnetic permeability	1.1
μ_∞	high-frequency magnetic permeability	1
ω_{om}	magnetic resonance angular frequency	$2\pi \cdot 9.2$ GHz
γ_m	magnetic damping factor	0.2 GHz

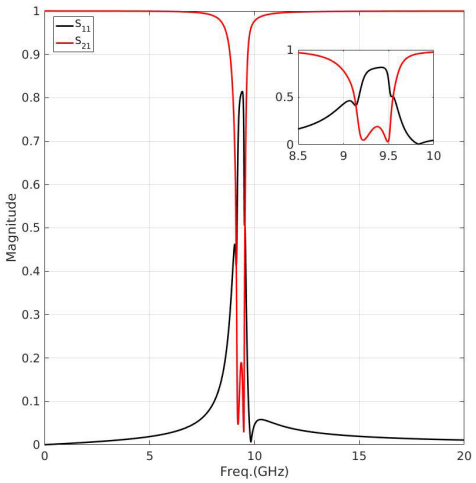

FIGURE 6. The magnitude of the scattering parameters for the NRI homogeneous slab with $d_{eff} = 2.5$ mm. The inset shows its behaviour magnified in the range [8.5, 10] GHz.

V. NUMERICAL EXPERIMENTS

In this section we elucidate the theoretical machinery discussed so far considering the problem of recovering the material parameters of two negative refractive index (NRI) homogeneous media slabs described by the following single resonance Lorentzian models [34], [46]:

$$\epsilon_r(\omega) = \epsilon_\infty + \frac{(\epsilon_s - \epsilon_\infty)\omega_{0e}^2}{\omega_{0e}^2 - \omega^2 + i\gamma_e\omega} \tag{59}$$

and

$$\mu_r(\omega) = \mu_\infty + \frac{(\mu_s - \mu_\infty)\omega_{0m}^2}{\omega_{0m}^2 - \omega^2 + i\gamma_m\omega} \tag{60}$$

The slabs are characterized by the same parameters, which are reported in Table (1), but they have different thickness; $d_{eff} = 2.5$ mm and $d_{eff} = 7.5$ mm, respectively. All the simulations have been carried out by using the Matlab software. The scattering parameters for these media have been obtained numerically using relations (1) and (2). Figures (6) and (7) show their magnitude and phase for the slab with thickness $d_{eff} = 2.5$ mm in the frequency ranges [0, 20] and [8.5, 10] GHz, respectively. This last one has been chosen to magnify these quantities around the slab dielectric and magnetic angular resonance frequencies. The S-parameters were

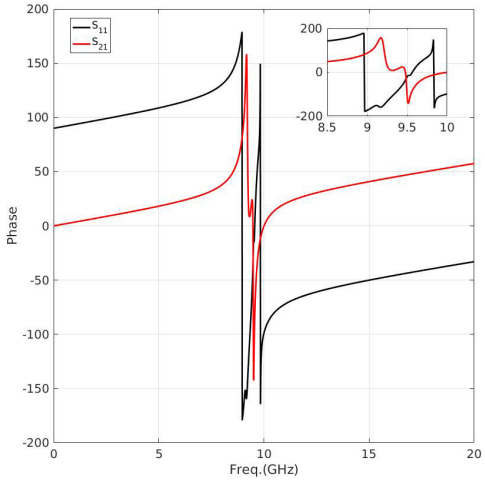

FIGURE 7. The phase of the scattering parameters for the NRI homogeneous slab with $d_{eff} = 2.5$ mm. The inset shows its behaviour magnified in the range [8.5, 10] GHz.

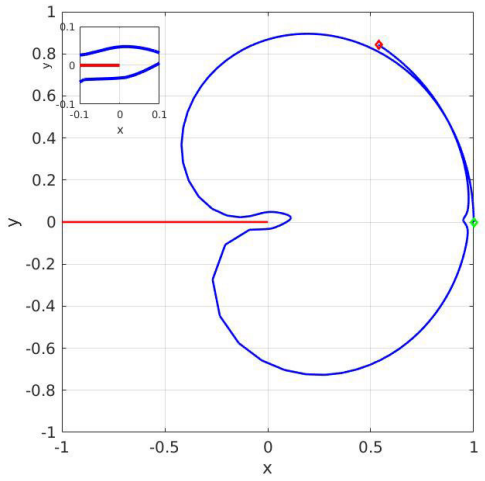

FIGURE 8. The path $\gamma(t) \triangleq S_{21}(\omega)/(1 - S_{11}(\omega)R_{01}(\omega))$ for the slab with $d_{eff} = 2.5$ mm. Green diamond marker: $\gamma(a)$, $a = 0$ Hz. Red diamond marker: $\gamma(b)$, $b = 20$ GHz. The inset shows the behaviour of $\gamma(t)$ magnified around the origin of $\dot{\mathbb{C}}$. Red continuous line: the ray $\mathbb{R}_\pi$.

sampled at 2048 points over the band [0, 20] GHz. Figure (8) shows the shape of $\gamma(t)$, given by (38), related to this case. The green diamond and red diamond markers locate the initial and final points of $\gamma(t)$, $\gamma(a), a = 0$ Hz, and $\gamma(b), b = 20$ GHz, respectively, showing as $\gamma(t)$ describes a counterclockwise curve on $\dot{\mathbb{C}}$ as the frequency increases. We can note as $\gamma(a)$ lies on $\mathbb{R}^+$, confirming the aforementioned remarks on its location. In addition, we can observe as no intersection exists between $\gamma(t)$ and the ray $\mathbb{R}_\pi$, that is, the branch cut of $log(\cdot)$. This implies that the pre-image of $\gamma(t)$, $\bar{\gamma}(t)$, must entirely lie in the half-open strip $(-\pi, \pi]$, that is the principal domain of univalence of $e^{(\cdot)}$.[2] As a consequence, the mapping

[2]We recall that the images of rectilinear semi-open strips of width 2π are overlapped on $\mathbb{C}$ by the mapping $e^{(\cdot)}$ (see figure (3)). If we consider a variable point w that describes a continuous counterclockwise (clockwise) path in $\mathbb{C}$, the corresponding image point $z = e^w$ traces a continuous counterclockwise (clockwise) path in $\dot{\mathbb{C}}$, which crosses the ray $\mathbb{R}_\pi$ every time the point w crosses the boundary between two adjacent strips [37].

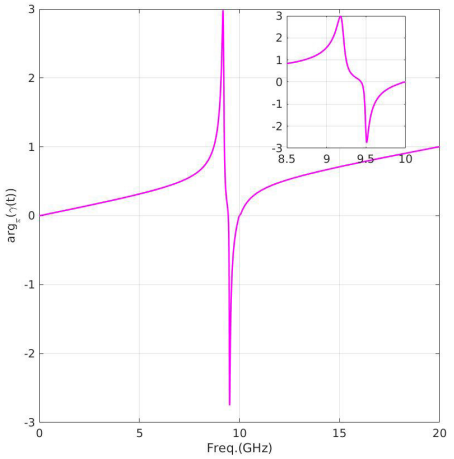

FIGURE 9. The argument function $arg_\pi(\gamma(t))$, $t \triangleq \omega \in [0, 20]$ GHz (continuous purple line). The inset shows its behavior magnified in the range [8.5, 10] GHz.

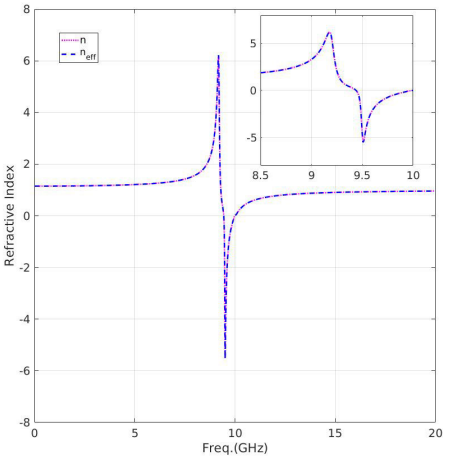

FIGURE 11. The refractive index $n(\omega)$ (dotted purple line), and the recovered effective refractive index $n_{eff}(\omega)$ (dashed blu line), for the NRI slab with $d_{eff} = 2.5$ mm. The inset shows the behaviour of these quantities magnified in the range [8.5, 10] GHz.

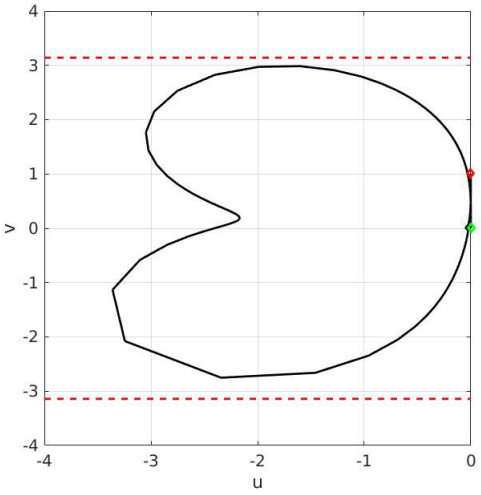

FIGURE 10. The pre-image of $\gamma(t)$, $\bar{\gamma}(t) = \mathsf{L}(\gamma(t))$ in $\mathbb{C}$. Green diamond marker: $\mathsf{L}(\gamma(a))$, $a = 0$ Hz. Red diamond marker: $\mathsf{L}(\gamma(b))$, $b = 20$ GHz. Red dotted lines: boundaries of the half-open rectilinear strip $(-\pi, \pi]$.

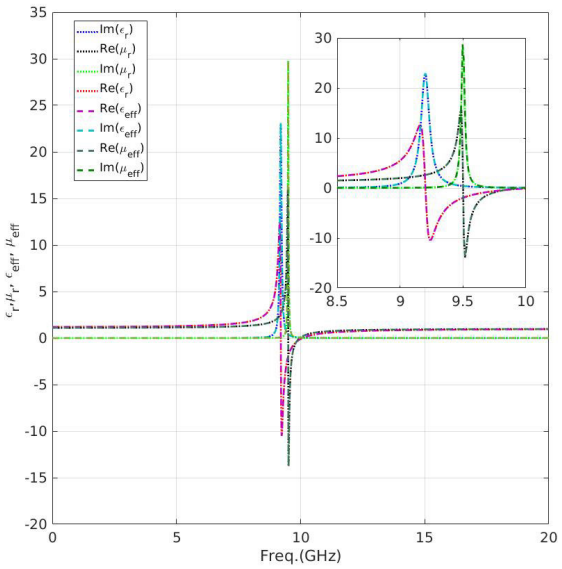

FIGURE 12. The real and imaginary part of $\epsilon_r(\omega)$ (red and blue dotted lines), $\mu_r(\omega)$ (green and black dotted lines), $\epsilon_{eff}(\omega)$ (purple and light blue dashed lines) and $\mu_{eff}(\omega)$ (light and dark green dashed lines) for the NRI slab with $d_{eff} = 2.5$ mm. The inset shows their behaviour magnified in the range [8.5, 10] GHz.

realized by (5) is bijective, and hence the inverse $f^{-1}(\cdot)$ exists, that is, the unique analytic logarithm of the Theorem 1, $\mathsf{L}(\cdot)$, coincides with $log(\cdot)$, which must be chosen as the first element of the chain (35) since it is the unique α-logarithm able to fulfill the constraint (36). All this allows to conclude that the slab sample with $d_{eff} = 2.5$ mm is electrically thin compared with the wavelength inside the medium within the $[0, 20]$ GHz band, and no branch ambiguity occur in this case. The imaginary part of $log(\gamma(t))$, the phase argument $arg_\pi(\gamma(t))$, depicted in Figure (9), is continuous over the frequency range, as expected from the considerations mentioned above. Figure (10) shows $\bar{\gamma}(t) = log(\gamma(t))$. The green diamond and red diamond markers indicate the initial and final points $log(\gamma(a))$ and $log(\gamma(b))$, respectively. The red dotted lines delimit the boundaries of the half-open rectilinear strip $(-\pi, \pi]$. We can note as $\bar{\gamma}(t)$ results entirely lying inside it, demonstrating the correctness of our theoretical analysis. Figure (11) shows a comparison between the exact refractive index $n(\omega) = \mathsf{Im}[\sqrt{\epsilon_r(\omega)\mu_r(\omega)}]$ and the recovered effective refractive index $n_{eff}(\omega)$ obtained solving (5) by $log(\cdot)$. In contrast, in figure (12) a comparison between exact $(\epsilon_r(\omega), \mu_r(\omega))$ and recovered $(\epsilon_{eff}(\omega), \mu_{eff}(\omega))$ constitutive parameters is depicted. The precise agreement among them is apparent. Figures (13) and (14) show the magnitude and phase of S_{11} and S_{21} for the 7.5 mm thickness slab in the range $[0, 20]$ GHz. Also, in the same figures is shown their behaviour magnified in the frequency band $[8.5, 10]$ GHz. For this case, the S-parameters were sampled at 16384 points

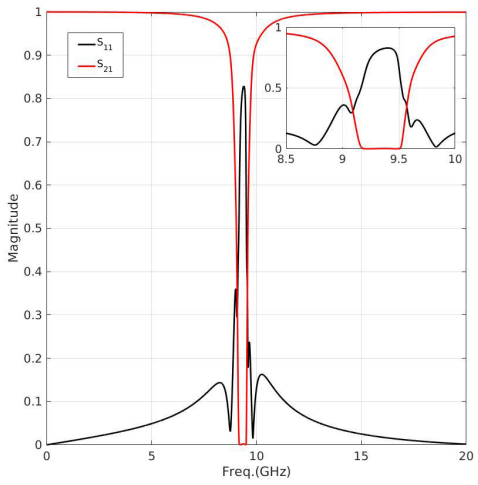

FIGURE 13. The magnitude of the scattering parameters for the NRI homogeneous slab with $d_{eff} = 7.5$ mm. The inset shows its behaviour magnified in the range [8.5, 10].

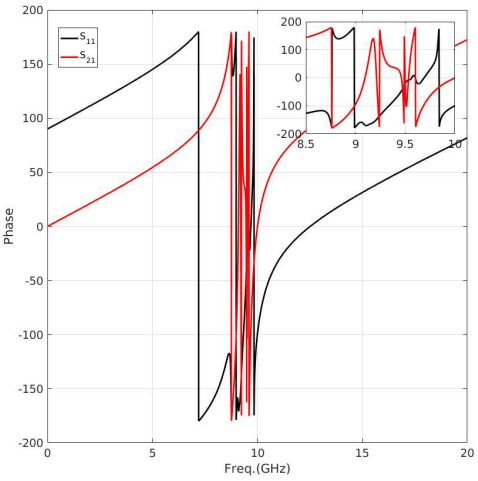

FIGURE 14. The phase of the scattering parameters for the NRI homogeneous slab with $d_{eff} = 7.5$ mm. The inset shows its behaviour magnified in the range [8.5, 10] GHz.

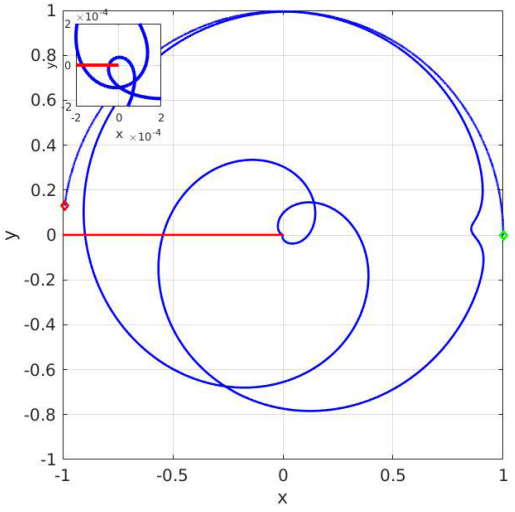

FIGURE 15. The path $\gamma(t) \triangleq S_{21}(\omega)/(1 - S_{11}(\omega)R_{01}(\omega))$ for the slab with $d_{eff} = 7.5$ mm. Green diamond marker: $\gamma(a)$, $a = 0$ Hz. Red diamond marker: $\gamma(b)$, $b = 20$ GHz. The inset shows its magnified around the origin of $\dot{\mathbb{C}}$. Red continuous line: the ray $\mathbb{R}_\pi$.

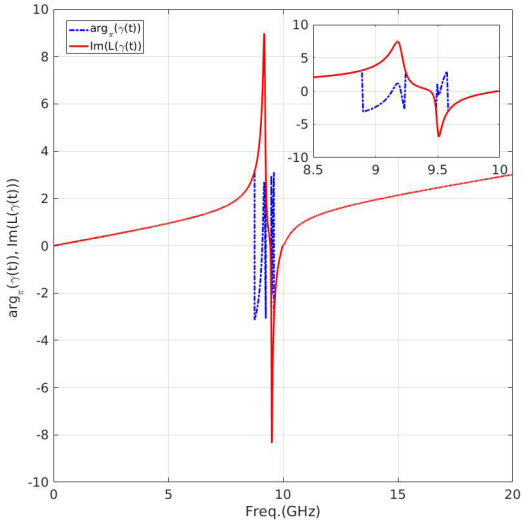

FIGURE 16. The argument function $arg_\pi(\gamma(t))$, (blue dash-dotted line) and the imaginary part of $\mathsf{L}(\gamma(t))$, $\mathsf{Im}[\mathsf{L}(\gamma(t))]$ (purple continuous line). The inset shows their behaviour magnified in the range [8.5, 10] GHz.

in the range [0, 20] GHz. We can note as the phase of the S-parameters results to be more rapidly changing than the previous case, suggesting the presence of the branch ambiguity issue, as pointed out in [22]. Hence, the slab sample with $d_{eff} = 7.5$ mm should be electrically thick compared with the wavelength inside the medium within the selected frequency band. This *ansatz* is confirmed by figure (15), which depicts the shape of the path (38) in $\dot{\mathbb{C}}$. In fact, unlike the 2.5 mm slab, we can observe that the path $\gamma(t)$ repeatedly intersects the ray $\mathbb{R}_\pi$. This clearly indicates that its pre-image, $\bar{\gamma}(t)$, does not lie exclusively inside the strip $(-\pi, \pi]$. Thus, on the contrary of the previous case $\mathsf{L}(\cdot) \neq log(\cdot)$, and the analytic continuation has to be employed to solve (5). Since the point $\gamma(a)$ (green diamond marker) lies on $\mathbb{R}^+$ (as it must), the principal logarithm $log(\cdot)$ can and must be used as the first element of the chain (35). We repeat once again that this choice is the only one guaranteeing the fulfilment of the constraint condition (36), essential to obtain a causal solution for $\mathsf{L}(\gamma(t))$, because $arg_\pi(\gamma(a)) = 0$. At this point, to realize the analytic continuation is suffice to evaluate $\mathsf{Im}[\mathsf{L}(\gamma(t))]$ making $arg_\pi(\gamma(t))$ continuous. Figure (16) shows the graph of $arg_\pi(\gamma(t))$ (dash-dotted blue line) over the frequency range [0, 20] GHz. The inset shows its behaviour magnified in the interval [8.5, 10] GHz. We can see as this function results characterized by four discontinuity points, that coincide with the number of intersection points between $\gamma(t)$ and $\mathbb{R}_\pi$. The same figure shows the graph of $\mathsf{Im}(\mathsf{L}(\gamma(t)))$ (purple continuous line) obtained by making continuous, i.e. unwrapping, $arg_\pi(\gamma(t))$ by using PUNWOS. Figure (17)

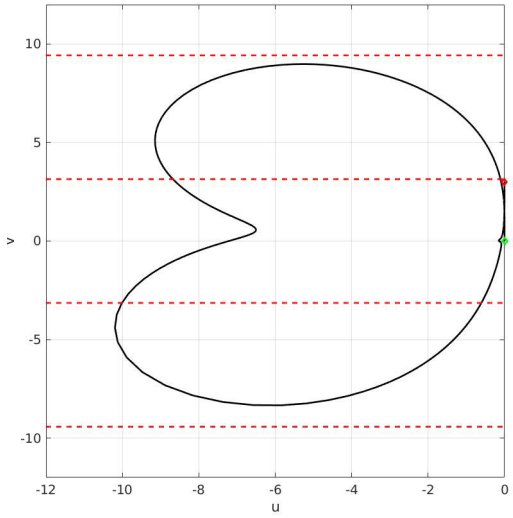

FIGURE 17. The pre-image of $\gamma(t)$, $\bar{\gamma}(t) = \mathsf{L}(\gamma(t))$ in $\mathbb{C}$. Green diamond marker: $\mathsf{L}(\gamma(a))$, $a = 0$ Hz. Red diamond marker: $\mathsf{L}(\gamma(b))$, $b = 20$ GHz. Red dotted lines: Boundaries of the half-open rectilinear strips $(-3\pi, -\pi]$, $(-\pi, \pi]$,and $(\pi, 3\pi]$.

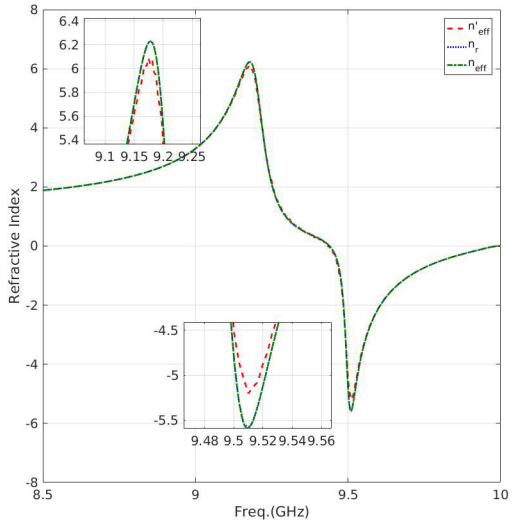

FIGURE 18. Refractive index $n(\omega)$ (dash-dotted green line), PUNWOS effective refractive index $n_{eff}(\omega)$ (dotted blu line), and K-K computed effective refractive index $n'_{eff}(\omega)$ (dashed red line) for the NRI slab with $d_{eff} = 7.5$ mm.

depicts $\bar{\gamma}(t) = \mathsf{L}(\gamma(t))$ for the 7.5 mm thickness slab. Also in this case, the green diamond and red diamond markers indicate the initial and final points $\mathsf{L}(\gamma(a))$ and $\mathsf{L}(\gamma(b))$, respectively. The red dotted lines represent the boundaries of the half-open rectilinear strips $(-3\pi, -\pi]$, $(-\pi, \pi]$, and $(\pi, 2\pi]$ in $\mathbb{C}$. On the contrary to 2.5 mm thick slab case, we can observe as $\bar{\gamma}(t)$ does not lie inside the $(-\pi, \pi]$ strip, as expected, demonstrating once again the correctness of our theoretical analysis. Figure (18) shows a comparison among the exact refractive index $n(\omega)$, the effective refractive index $n_{eff}(\omega)$, recovered by using PUNWOS, and the effective refractive index $n'_{eff}(\omega)$, computed by using the numerical

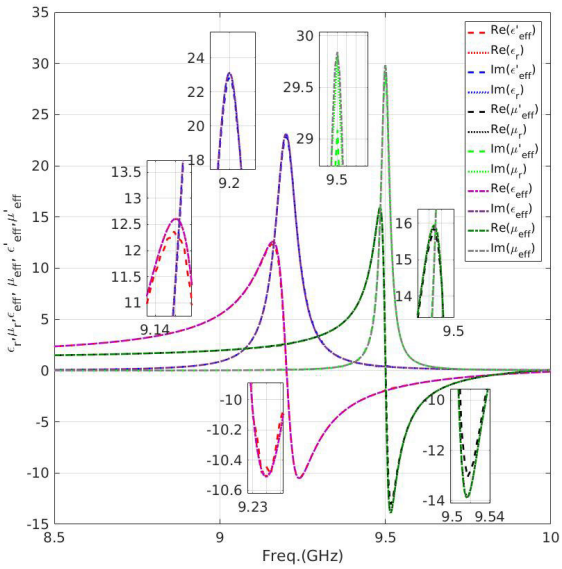

FIGURE 19. The real and imaginary part of $\epsilon_r(\omega)$ (red and blue dotted lines), $\mu_r(\omega)$ (green and black dotted lines), $\epsilon_{eff}(\omega)$ (ligh and dark purple dash-dotted lines), $\mu_{eff}(\omega)$ (dark green and gray dash-dotted lines), $\epsilon'_{eff}(\omega)$ (red and dark blue dashed lines), and $\mu'_{eff}(\omega)$ (black and green dashed lines) for the NRI slab with $d_{eff} = 7.5$ mm. The insets shows their behaviour magnified around the peaks.

implementation of the Kronig-Kramers approach described in [23], in the frequency range [8.5, 10] GHz. The insets report the behaviour of these quantities around their peaks. Finally, the figure (17) shows the comparison among the real and imaginary part of the couples $(\epsilon_{eff}(\omega), \mu_{eff}(\omega))$, $(\epsilon'_{eff}(\omega), \mu'_{eff}(\omega))$, the first recovered by PUNWOS, while the second computed by the Kronig-Kramers relations, and the couple of exact parameters $(\epsilon_r(\omega), \mu_r(\omega))$, respectively, in the same frequency range as for the refractive index. In contrast, the insets depict the behaviour of these quantities in correspondence to their peaks. The results obtained show an excellent agreement among PUNWOS and Kronig-Kramers method, as theoretically expected.

VI. CONCLUSION

In this study, we rigorously demonstrated that the NWR branch ambiguity issue can be avoided by computing the proper right-inverse of the relationship (5) through the analytic continuation of a suitable analytic logarithm along the path determined in the complex plane by the scattering parameters of the MM under analysis. This prolongation has to be realized according to the formulation provided by Theorem 1, which states the conditions so that we can determine a unique solution for this problem. Accordingly, the choice of $log(\cdot)$ as the first element of the chain of the analytic function elements constituting this right inverse. i.e. the analytic logarithm $\mathsf{L}(\cdot)$, has been demonstrated in terms of the Fourier inverse transform property of the complex refraction index $N_{eff}(\omega)$. Furthermore, the equivalence between analytic continuation and the PUNWOS method was proved. To this end, considering that PUNWOS is a technique

introduced for homomorphic signal processing, we showed that the relationship between the sub-systems' input-output functions $\phi_{\mathcal{H}'}(\cdot)$ and $\phi_{\mathcal{H}''}(\cdot)$ of the canonical homomorphic system for multiplication, $\mathcal{C}$, is analogous to that which links $\mathsf{L}(\cdot)$ and $e^{(\cdot)}$ in the case of the NWR retrieval method and that PUNWOS can evaluate $\mathsf{L}(\cdot)$. Based on this result, the relationship between PUNWOS and the Kronig-Kramers relations was also demonstrated. To enlighten all the above mentioned theoretical points, we have carried out some numerical experiments related to recovering the effective parameters of a couple of NRI media. From a numerical point of view, the very close agreement we have obtained between the PUNWOS and the Kronig-Kramers computational results demonstrate the effectiveness of the theoretical analysis conducted in this study. Future work will be devoted to using the concepts of global analytic functions and Riemann surfaces in the field of the effective parameters recovering by NRW method [37]. We conclude by pointing out that our work opens the possibility to employ the vast theoretical equipment developed in the phase unwrapping field to achieve the retrieval of MMs' effective parameters by following the NWR method when this kind of characterization is permitted [16], [17].

REFERENCES

[1] C. Simovski and S. & Tretyakov, *An Introduction to Metamaterials Nanophotonics*. Cambridge, U.K.: Cambridge Univ. Press, 2020.
[2] T. J. Cui, W. X. Tang, X. M. Yang, Z. L. Mei, and W. X. Jiang, *Metamaterials: Beyond Crystals, Noncrystals, Quasicrystals*. Boca Raton, FL, USA: CRC Press, 2017.
[3] X. Fu and T. J. Cui, "Recent progress on metamaterials: From effective medium model to real-time information processing system," *Prog. Quantum Electron.*, vol. 67, Sep. 2019, Art. no. 100223.
[4] A. K. Iyer, A. Alu, and A. Epstein, "Metamaterials and metasurfaces—Historical context, recent advances, and future directions," *IEEE Trans. Antennas Propag.*, vol. 68, no. 3, pp. 1223–1231, Mar. 2020.
[5] S. Lee, S. Baek, T. Kim, H. Cho, S. Lee, J. Kang, and B. Min, "Metamaterials for enhanced optical responses and their application to active control of terahertz waves," *Adv. Mater.*, vol. 32, no. 35, Sep. 2020, Art. no. 2000250.
[6] Y. T. Aladadi and M. A. S. Alkanhal, "Classification and characterization of electromagnetic materials," *Sci. Rep.*, vol. 10, no. 1, pp. 1–11, Dec. 2020.
[7] D. R. Smith, S. Schultz, P. Markoš, and C. M. Soukoulis, "Determination of effective permittivity and permeability of metamaterials from reflection and transmission coefficients," *Phys. Rev. B, Condens. Matter*, vol. 65, no. 19, Apr. 2002, Art. no. 195104.
[8] D. R. Smith, D. C. Vier, T. Koschny, and C. M. Soukoulis, "Electromagnetic parameter retrieval from inhomogeneous metamaterials," *Phys. Rev. E, Stat. Phys. Plasmas Fluids Relat. Interdiscip. Top.*, vol. 71, no. 3, Mar. 2005, Art. no. 036617.
[9] L. F. Chen, C. K. Ong, C. P. Neo, V. V. Varadan, and V. K. Varadan, *Microwave Electronics: Measurement and Materials Characterization*. Hoboken, NJ, USA: Wiley, 2004.
[10] H. Li, X. Man, and J. Qi, "Accurate and robust characterization of metasurface-enabled frequency reconfigurable antennas by radially homogeneous model," *IEEE Access*, vol. 7, pp. 122605–122612, 2019.
[11] S. Hannan, M. T. Islam, A. F. Almutairi, and M. R. I. Faruque, "Wide bandwidth angle-and polarization-insensitive symmetric metamaterial absorber for X and Ku band applications," *Sci. Rep.*, vol. 10, no. 1, pp. 1–9, 2020.
[12] T. A. Elwi, "Printed microwave metamaterial-antenna circuitries on nickel oxide polymerized palm fiber substrates," *Sci. Rep.*, vol. 9, no. 1, pp. 1–14, Dec. 2019.
[13] F. B. Ashraf, T. Alam, and M. T. Islam, "A uniplanar left-handed metamaterial for terrestrial microwave links," *IEEE Microw. Wireless Compon. Lett.*, vol. 28, no. 2, pp. 108–110, Feb. 2018.
[14] M. Rashedul Islam, M. Tariqul Islam, M. Moniruzzaman, M. Samsuzzaman, B. Bais, H. Arshad, and G. Muhammad, "Square enclosed circle split ring resonator enabled epsilon negative (ENG) near zero index (NZI) metamaterial for gain enhancement of multiband satellite and radar antenna applications," *Results Phys.*, vol. 19, Dec. 2020, Art. no. 103556.
[15] E. Ekmekci, U. Kose, A. Cinar, O. Ertan, and Z. Ekmekci, "The use of metamaterial type double-sided resonator structures in humidity and concentration sensing applications," *Sens. Actuators A, Phys.*, vol. 297, Oct. 2019, Art. no. 111559.
[16] C. R. Simovski, "Material parameters of metamaterials (a Review)," *Opt. Spectrosc.*, vol. 107, no. 5, pp. 726–753, Nov. 2009.
[17] C. R. Simovski, "On electromagnetic characterization and homogenization of nanostructured metamaterials," *J. Opt.*, vol. 13, no. 1, Jan. 2011, Art. no. 013001.
[18] S. Arslanagic, T. V. Hansen, N. A. Mortensen, A. H. Gregersen, O. Sigmund, R. W. Ziolkowski, and O. Breinbjerg, "A review of the scattering-parameter extraction method with clarification of ambiguity issues in relation to metamaterial homogenization," *IEEE Antennas Propag. Mag.*, vol. 55, no. 2, pp. 91–106, Apr. 2013.
[19] X. Chen, T. M. Grzegorczyk, B.-I. Wu, J. Pacheco, and J. A. Kong, "Robust method to retrieve the constitutive effective parameters of metamaterials," *Phys. Rev. E, Stat. Phys. Plasmas Fluids Relat. Interdiscip. Top.*, vol. 70, no. 1, Jul. 2004, Art. no. 016608.
[20] Y. Shi, Z.-Y. Li, K. Li, L. Li, and C.-H. Liang, "A retrieval method of effective electromagnetic parameters for inhomogeneous metamaterials," *IEEE Trans. Microw. Theory Techn.*, vol. 65, no. 4, pp. 1160–1178, Apr. 2017.
[21] O. Luukkonen, S. I. Maslovski, and S. A. Treyakov, "A stepwise Nicolson–Ross–Weir-based material parameter extraction method," *IEEE Antennas Wireless Propag. Lett.*, vol. 10, pp. 1295–1298, 2011.
[22] Z. Szabo, G. H. Park, R. Hedge, and E. P. Li, "A unique extraction of metamaterial parameters based on Kramers–Kronig relationship," *IEEE Trans. Microw. Theory Techn.*, vol. 58, no. 10, pp. 2646–2653, Oct. 2010.
[23] Z. Szabó, "Closed form Kramers–Kronig relations to extract the refractive index of metamaterials," *IEEE Trans. Microw. Theory Techn.*, vol. 65, no. 4, pp. 1150–1159, Apr. 2017.
[24] V. V. Varadan and R. Ro, "Unique retrieval of complex permittivity and permeability of dispersive materials from reflection and transmitted fields by enforcing causality," *IEEE Trans. Microw. Theory Techn.*, vol. 55, no. 10, pp. 2224–2230, Oct. 2007.
[25] G. Angiulli, M. Versaci, S. Calcagno, and P. Di Barba, "Quick retrieval of effective electromagnetic metamaterial parameters by using a multi-fidelity surrogate modelling approach," *Eur. Phys. J. Appl. Phys.*, vol. 90, no. 2, p. 20901, May 2020.
[26] S. Yoo, S. Lee, J.-H. Choe, and Q.-H. Park, "Causal homogenization of metamaterials," *Nanophotonics*, vol. 8, no. 6, pp. 1063–1069, May 2019.
[27] A. Oppenheim and R. W. Schafer, *Discrete Time Signal Processing*. Upper Saddle River, NJ, USA: Prentice-Hall, 2009.
[28] J. J. Barroso and U. C. Hasar, "Constitutive parameters of a metamaterial slab retrieved by the phase unwrapping method," *J. Infr., Millim., Terahertz Waves*, vol. 33, no. 2, pp. 237–244, Feb. 2012.
[29] Z. X. Cao, F. G. Yuan, and L. H. Li, "An automated phase correction algorithm for retrieving permittivity and permeability of electromagnetic metamaterials," *AIP Adv.*, vol. 4, no. 6, Jun. 2014, Art. no. 067115.
[30] Y. Shi, Z.-Y. Li, L. Li, and C.-H. Liang, "An electromagnetic parameters extraction method for metamaterials based on phase unwrapping technique," *Waves Random Complex Media*, vol. 26, no. 4, pp. 417–433, Oct. 2016.
[31] U. C. Hasar, A. Muratoglu, M. Bute, J. J. Barroso, and M. Ertugrul, "Effective constitutive parameters retrieval method for bianisotropic metamaterials using waveguide measurements," *IEEE Trans. Microw. Theory Techn.*, vol. 65, no. 5, pp. 1488–1497, May 2017.
[32] Y. T. Aladadi and M. A. S. Alkanhal, "Extraction of metamaterial constitutive parameters based on data-driven discontinuity detection," *Opt. Mater. Exp.*, vol. 9, no. 9, p. 3765, 2019.
[33] H, M. Nussenzveig, *Causality and Dispersion Relations*. New York, NY, USA: Academic, 1972.
[34] K.-E. Peiponen, V. Lucarini, E. M. Vartiainen, and J. J. Saarinen, "Kramers-kronig relations and sum rules of negative refractive index media," *Eur. Phys. J. B*, vol. 41, no. 1, pp. 61–65, Sep. 2004.
[35] J. J. Barroso and U. C. Hasar, "Comments on 'A unique extraction of metamaterial parameters based on Kramers–Kronig relationship,'" *IEEE Trans. Microw. Theory Techn.*, vol. 60, no. 6, pp. 1743–1744, Jun. 2012.

[36] Z. Szabo, G. H. Park, R. Hedge, and E. P. Li, "Authors' reply to 'comments on unique extraction of metamaterial parameters based on Kramers–Kronig relationship,'" *IEEE Trans. Microw. Theory Techn.*, vol. 60, no. 11, pp. 3634–3635, Nov. 2012.
[37] A. I. Markushevich, *Theory of Functions of a Complex Variable*, 2nd ed. New York, NY, USA: Chelsea Publishing Company, 1985.
[38] B. P. Palka, *An Introduction to Complex Function Theory*. New York, NY, USA: Springer-Verlag, 1991.
[39] E. Suhubi, *Functional Analysis*. Basingstoke, U.K.: Springer Nature, 2010.
[40] R. H. Dyer and D. E. Edmunds, *From Real to Complex Analysis*. Dordrecht, The Netherlands: Springer, 2014.
[41] E. Wegert, *Visual Complex Functions: An Introduction with Phase Portraits*. Cham, Switzerland: Springer, 2012.
[42] R. Bracewell, *The Fourier Transform and Its Applications*. New York, NY, USA: McGraw-Hill, 2000.
[43] A. Oppenheim, R. Schafer, and T. Stockham, "Nonlinear filtering of multiplied and convolved signals," *IEEE Trans. Audio Electroacoustics*, vol. 16, no. 3, pp. 437–466, Sep. 1968.
[44] T. F. Quatieri, *Discrete-Time Speech Signal Processing: Principles and Practice*. London, U.K.: Pearson, 2006.
[45] W. K. Chen, *Broadband Matching: Theory and Implementations*. Singapore: World Scientific, 2015.
[46] R. W. Ziolkowski and E. Heyman, "Wave propagation in media having negative permittivity and permeability," *Phys. Rev. E, Stat. Phys. Plasmas Fluids Relat. Interdiscip. Top.*, vol. 64, no. 5, Oct. 2001, Art. no. 056625.

GIOVANNI ANGIULLI (Senior Member, IEEE) received the Laurea (master's) degree in computer science engineering from the University of Calabria, Italy, in 1993, and the Ph.D. degree in electronics and computer science engineering from the University of Napoli Federico II, Italy, in 1998. Since 1999, he has been with the Department of Information, Infrastructures, and Sustainable Energy (DIIES) (formerly, DIMET), Mediterranea University of Reggio Calabria, Italy, as an Adjunct Professor. He worked on microwave imaging to detect female breast tumours and ground-penetrating radar applications in cultural heritage in the later years. His main research interests include computational electromagnetics, group theory methods, and surrogate modeling techniques applied in electromagnetics and electrical engineering. He has been an IEICE member, since 2013. He has been honoured as an Outstanding Associate Editor, for the year 2018, by the IEEE Access Editorial Board in recognition of his exceptional contributions. He currently serves as an Associate Editor for IEEE Access and an Academic Editor for *PeerJ Computer Science*. He served as a Guest Editor for *Mathematics* (MDPI) Special Issue on "Surrogate modeling and related methods in science and engineering."

MARIO VERSACI (Senior Member, IEEE) received the degree in civil engineering from the Mediterranea University of Reggio Calabria, Italy, in 1994, the Ph.D. degree in electronic engineering from the Mediterranea University of Reggio Calabria, in 1999, and the Laurea degree in mathematics from the University of Messina, Italy, in 2013. He currently serves as an Associate Professor of electrical engineering with the Mediterranea University of Reggio Calabria, where he serves as the Scientific Head of the NDT/NDE Laboratory. His research interests include soft computing techniques for NDT/NDE and image processing. He is a member of the Italian Society for Industrial and Applied Mathematics.